A Domain Decomposition Method for Silicon Devices

Carlo Cercignani,[*] Irene M. Gamba,[†] Joseph W. Jerome,[‡] and Chi-Wang Shu[§]

Abstract

A mesoscopic/macroscopic model for self-consistent charged transport under high field scaling conditions corresponding to drift-collisions balance was derived by Cercignani, Gamba, and Levermore in [4]. The model was summarized in relationship to semiconductors in [2]. In [3], a conceptual domain decomposition method was implemented, based upon use of the drift-diffusion model in highly-doped regions of the device, and use of the high-field model in the channel, which represents a (relatively) lightly-doped region. The hydrodynamic model was used to calibrate interior boundary conditions. The material parameters of GaAs were employed in [3].

This paper extends the approach of [3].

- Benchmark comparisons are described for a Silicon $n^+ - n - n^+$ diode. A global kinetic model is simulated with Silicon parameters. These simulations are sensitive to the choice of mobility/relaxation.

- An elementary global domain decomposition method is presented. Mobilities are selected consistently with respect to the kinetic model.

This study underscores the significance of the asymptotic parameter η defined below, as the ratio of drift and thermal velocities as a way to measure the change in velocity scales. This parameter gauges the effectiveness of the high field model.

[*]Politecnico di Milano, 20133 Milano, Italy.
tel: 0039-2-23994557, Fax: 0039-2-23994568, email: carcer@mate.polimi.it
[†]Department of Mathematics and Texas Institute of Computational and Applied Mathematics, University of Texas, Austin, TX 78712.
tel: (512) 471-7150, Fax: (512) 471-9038, email: gamba@math.utexas.edu
[‡]Department of Mathematics, Northwestern University, Evanston, IL 60208.
tel: (847) 491-5575, Fax: (847) 491-8906, email: jwj@math.nwu.edu; corresponding author.
[§]Division of Applied Mathematics, Brown University, Providence, RI 02912.
tel: (401) 863-2549, Fax: (401) 863-1355, email: shu@cfm.brown.edu

1 Introduction

In previous work [2], the authors introduced a conceptual domain decomposition approach, combining drift-diffusion, kinetic, and high-field regimes. The high-field model had been introduced in [4]. The approach was implemented in preliminary form in [3]. More precisely, the hydrodynamic model was used as a global calibrator (see also [9, 10]), and used to define internal boundary conditions, separating drift-diffusion from high-field regions. In particular, it was found that this methodology allowed for a validation of the high-field model in the channel region for devices described by material parameters of GaAs. In this paper, we continue the program begun in [2, 3], as applied to devices described by Silicon material parameters. We again define a global calibrator, a linear approximation to the Boltzmann transport equation, and solve this in one space and one velocity dimension. In the process, we compare this global calibrator with the drift-diffusion model, and explore the role of mobility coefficients in the matching.

Second, we implement an elementary global domain decomposition method. Mobilities are selected consistently with respect to the kinetic model. The simulations depend fundamentally upon the mobilities selected.

The differences which are found via use of the high field model are less pronounced than those found in [3] for GaAs devices. This is not surprising, in view of the narrower range for Silicon of the critical parameter, η, defined below as the ratio of the drift and thermal velocities. This parameter, exhibited in Fig. 5.2, gauges the effectiveness of the high field model as explained below.

We have followed the spirit of Fatemi and Odeh, who simulated the linear Boltzmann equation in [5], for the kinetic computations.

2 Models Employed in This Paper

The following models are used in this paper.

2.1 The Kinetic Model

The one-dimensional kinetic model can be written as follows:

$$\frac{\partial f(x,u,t)}{\partial t} + u\frac{\partial f(x,u,t)}{\partial x} - \frac{e}{m}E(x,t)\frac{\partial f(x,u,t)}{\partial u} = \frac{n(x,t)M(u) - f(x,u,t)}{\tau}, \tag{2.1}$$

where

$$M(u) = \frac{1}{\sqrt{2\pi\theta}}e^{-\frac{u^2}{2\theta}} \tag{2.2}$$

is a Maxwellian, with

$$\theta = \frac{k_b}{m}T_0. \tag{2.3}$$

Values for e, m, k_b, and T_0 are given at the conclusion of §3. The concentration $n(x,t)$ is obtained by

$$n(x,t) = \int_{-\infty}^{\infty} f(x,u,t)\,du. \tag{2.4}$$

Also, the electric field $E(x,t)$ is obtained by solving the coupled potential equation,

$$E(x,t) = -\phi_x, \qquad (\epsilon\phi_x)_x = e(n - n_d), \tag{2.5}$$

with the boundary conditions

$$\phi(0, t) = 0, \qquad \phi(L, t) = vbias, \tag{2.6}$$

with $L = 0.6\mu m$, and the relaxation parameter τ is computed by

$$\tau = \frac{m\mu}{e}. \tag{2.7}$$

μ is the mobility and we have the following characterizations.

1. Constant μ. We have used the values:

$$\mu = 0.1323 \, \mu m^2/(V \, ps), \tag{2.8}$$

$$\mu = 0.0367 \, \mu m^2/(V \, ps). \tag{2.9}$$

2. Variable μ depending on the doping n_d:

$$\mu = \begin{cases} 0.0367 \, \mu m^2/(V \, ps), & \text{in the } n^+ \text{ region,} \\ 0.1323 \, \mu m^2/(V \, ps), & \text{in the } n \text{ region.} \end{cases} \tag{2.10}$$

In fact, the formula

$$\mu(n_d(x)) = 0.0088 \left(1.0 + \frac{14.2273}{1.0 + \frac{n_d(x)}{143200}} \right), \tag{2.11}$$

where n_d is in the unit of $1/\mu m^3$, which is more general, is used here.

3. Variable μ depending on the electric field E, used in drift-diffusion simulations to model saturation (see [7]):

$$\mu(E) = 2\mu_0 / \left[1 + \sqrt{1 + 4(\mu_0|E|/v_d)^2} \right], \tag{2.12}$$

where

$$\mu_0 = 0.1323 \, \mu m^2/(V \, ps), \qquad v_d = 0.13 \, \mu m/ps. \tag{2.13}$$

v_d here is taken to be the maximum of the velocity in the hydrodynamic run with $vbias = 1.5$ and $\mu = \mu(n_d)$ as given by (2.10) (see [8]), which was calibrated by Monte-Carlo simulations.

2.2 The Drift-Diffusion (DD) Model.

The drift-diffusion (DD) model is well documented (see, for example, [7]). It is given by:

$$n_t + J_x = 0, \tag{2.14}$$

where

$$J = J_{hyp} + J_{vis},$$

and

$$J_{hyp} = -\mu n E,$$
$$J_{vis} = -\tau(n\theta)_x.$$

2.3 The High-Field (HF) Model.

The model can be written as follows:

$$n_t + J_x = 0, \tag{2.15}$$

where

$$J = J_{hyp} + J_{vis},$$

and

$$J_{hyp} = -\mu n E + \tau\mu\left(\frac{e}{\epsilon}\right)n(-\mu n E + \omega),$$

$$J_{vis} = -\tau[n(\theta + 2\mu^2 E^2)]_x + \tau\mu E(\mu n E)_x.$$

For our current one dimensional case, ω is taken to be a constant:

$$\omega = (\mu n E)|_{x=0}.$$

The model is developed in [4] by asymptotic expansion methods (Chapman-Enskog) for the kinetic formulation of the problem (2.1)–(2.5), under strong forcing scaling assumptions that correspond to a drift-collisions balance regime.

An ad-hoc version of this model was first proposed by Thornber [16] for a given field. Thornber's equations, not quite as in the form above, are also called 'Augmented Drift-Diffusion' equations and were computed in [12]. Simulations of doped devices using Thornber's equations are known to be unsatisfactory due to the fact that they cannot be used to model highly doped regions, where the dominant scaling yields drift diffusion models.

Later, Trugman and Taylor [17] proposed the study of drift-collision balance regimes as a regime corresponding to non–equilibrium due to inhomogeneities of small devices and worked out a one dimensional case for a relaxation model. Frosali, Paveri-Fontana and Van der Meer [6] extended [17] for the 3-dimensional case, and studied the stability of the kinetic solution in the space homogeneous case. Poupaud (see [13] and [14]) solved the balance equation in the 3-dimensional case for a general linear collision operator and a given field. He found solvability conditions to avoid runaway phenomena and computed the corresponding Hilbert expansion and provided some a priori estimates. Finally, the authors of [4] computed the self-consistent Chapman-Enskog expansion for the relaxation model via a recursion formula. As a consequence, the self-consistent modes allow changes in homogeneities in the field scales, and thus bring to light the need for domain decomposition techniques.

The development of [4] requires three dimensionless parameters, viz. ,

- The ratio η of drift and free velocity (the latter usually taking on the thermal velocity):

$$\eta = U/\overline{\theta}^{1/2}, \tag{2.16}$$

  where U, in units of velocity, is given by

$$\frac{\tau e}{m}\frac{[\phi]}{L},$$

  for a length scale L and a potential drop $[\phi]$;

- The scaled mean free path ε:

$$\varepsilon = \frac{\tau\overline{\theta}^{1/2}}{L}; \tag{2.17}$$

4

- The scaled Debye length γ from the electrostatic potential equation of a self-consistent model:

$$\gamma = \frac{\bar{\rho} e L^2}{\epsilon[\phi]}, \tag{2.18}$$

where $\bar{\rho}$ scales the density of the fixed background $n_d(x)$.

For η of the same order of ε and both very small as in the highly doped regions, the Chapman-Enskog expansion associated with system (2.1)–(2.5) yields the DD equations (2.14). However, inside the channel region, η becomes of order of one as well as γ. Here the corresponding expansion yields the high-field model (2.15).

3 Simulation

The device we consider for this paper is the one dimensional Silicon n^+-n-n^+ structure of length $0.6\mu m$. The device used is as follows: $x \in [0, 0.6]$; the doping is defined by $n_d(x) = 5 \times 10^5/\mu m^3$ in $0 \le x \le 0.1$ and in $0.5 \le x \le 0.6$, and by $n_d(x) = 2 \times 10^3/\mu m^3$ in $0.15 \le x \le 0.45$, with a smooth intermediate transition. This is the Silicon device analogue of the GaAs device used by Baranger and Wilkins [1], except for a smooth transition of width $0.05\mu m$ at the junctions.

More specific conditions for various models are listed below.

1. For the kinetic model (2.1):

   - The velocity space is artificially cut at

   $$-a \le u \le a, \tag{3.1}$$

   where we monitor to ensure that $f(x, u, t)$ is always very small at the boundary $u = \pm a$ for the final steady state results. We learned that it is more than enough in all our runs to use $a = 3.5$.
   - We use a uniform grid both in x and in u, with 160×150 points.
   - At $x = 0$, take

   $$f(0, u, t) = n_d(0) M(u) \tag{3.2}$$

   if $u \ge 0$, and no boundary condition (extrapolation of the numerical solution from inside the domain to the boundary) if $u < 0$. Also take $\phi(0, t) = 0$.
   - At $x = 0.6$, take

   $$f(0.6, u, t) = n_d(0.6) M(u) \tag{3.3}$$

   if $u \le 0$, and no boundary condition (extrapolation of the numerical solution from inside the domain to the boundary) if $u > 0$. Also take $\phi(0.6, t) = vbias$.
   - At $u = -a$ and $u = a$, take no boundary condition (extrapolation of the numerical solution from inside the domain to the boundary).

2. For the elementary domain decomposition, we apply the low field drift-diffusion (DD) model (2.14) in [0,A] and [B,0.6], and the high-field (HF) model (2.15) in (A,B). For a fixed pair (A,B), we perform the following:

   - We use a uniform grid in x with 160 points.

- At $x = 0$ and $x = 0.6$, take the boundary conditions

$$n(0, t) = n_d(0), \, \phi(0, t) = 0,$$

$$n(0.6, t) = n_d(0.6), \, \phi(0.6, t) = vbias.$$

- At the interfaces $x = A$ and $x = B$, there are no explicit interface boundary conditions. The coupling of the drift-diffusion model and the high field model is through the ghost points used in the computation:
  - When a grid point is inside [0,A] or [B,0.6], the solution n is updated by the drift-diffusion model (2.14) using a fifth order conservative WENO scheme. Since this scheme has a 7-point stencil, when computing the updates near the interfaces A or B, the stencil actually goes into the region (A,B), hence the information in that high field region is used.
  - Similarly, the high field model (2.15) is used to update the solution if the grid point is inside (A,B). Again, the 7-point stencil of the numerical scheme implies that information inside the drift-diffusion region [0,A] and [B,0.6] is used when the grid point is near the interfaces A and B.

Simulations are performed for $vbias$ from 0V to 1.5V, and results are shown only for $vbias = 1.5$V to save space. Other parameters: $m = 0.26 \times 0.9109 \, (10^{-30} Kg)$, $e = 0.1602 \, (10^{-18} C)$, $k_b = 0.138046 \times 10^{-4} \, (10^{-18} J/Kelvin)$, $\epsilon = 11.7 \times 8.85418 \, (10^{-18} F/\mu m)$, $T_0 = 300K$.

4   Numerical Algorithm

We use the ENO schemes developed in [15] and the weighted ENO (WENO) schemes developed in [11]. ENO and WENO schemes are designed for hyperbolic conservation laws or other problems containing either discontinuous solutions or solutions with sharp gradients. The guiding principle is an adaptive local choice of a stencil (ENO), or use of a nonlinear convex combination of contributions from local stencils (WENO), so that contributions from stencils containing a possible discontinuity or other unpleasant features (e.g., a high gradient) are either completely avoided (ENO) or are assigned a nearly zero weight (WENO). In doing this, uniform high order accuracy can be achieved without introducing any oscillations near discontinuities or sharp gradient regions. The high order accuracy of these algorithms allows us to use relatively coarse grids and still get very accurate results. The algorithms are extremely stable and robust in all the numerical simulations.

5   Simulation Results

In all the numerical simulations, we perform a long time integration until a steady state is reached.

In Fig. 5.1, Fig. 5.2 and Fig. 5.3 we show the results of the kinetic simulation for $vbias = 1.5$ volt with various forms of mobility μ, given by (2.8), (2.9), (2.10) and (2.12). Fig. 5.1 contains the results of concentration n, velocity v

$$v(x, t) = \int_{-\infty}^{\infty} u f(x, u, t) du \, / \, n(x, t), \tag{5.1}$$

electric field E and potential ϕ. Fig. 5.2 contains the results of the I-V curve with

$$I = \frac{e}{b - a} \int_a^b n(x, t) v(x, t) dx. \tag{5.2}$$

6

Notice that the collision integrals conserve particle number, hence $n(x,t)v(x,t)$ should be a constant in steady states. We still take the average in (5.2) in the whole region $[a,b]=[0, 0.6]$ to compute I. The quantity η for $vbias = 1.5V$, defined in (2.16), which is useful for the verification of suitability for the high-field model (see Section 2.3), is also plotted in Fig. 5.2. Fig. 5.3 contains the probability density function $f(x,u,t)/n(x,t)$ at $x = 0.12$ and $x = 0.42$.

For this channel, at $vbias = 1.5V$, the scaled mean free path ε defined in (2.17) is in the range of 0.01 to 0.07, depending on the mobility assumptions.

From Fig. 5.1, Fig. 5.2 and Fig. 5.3 we can see that different mobility assumptions yield significantly different results, especially in velocity, and hence also affect the I-V curves. This indicates that, when using kinetic results as benchmarks, one must be careful in the mobility assumptions. Comparing with the simulation results of the hydrodynamic model in [8], which is calibrated by Monte-Carlo simulations, we can see that the choices (2.8), (2.9) and (2.10) for the mobility produce results over-estimating the velocity, while the choice (2.12) is producing velocity at the correct magnitude. The over-estimation of the velocity, when the more physical mobility assumption (2.10) is used, has also been observed, to a lesser extent, in the work of Fatemi and Odeh [5], where two space dimensions are used in the phase space for the kinetic model. Presumably this over-estimation is an indication that the collision model used in the kinetic model is over-simplified. Henceforth, we will concentrate our attention on the field dependent mobility $\mu = \mu(E)$ as given by (2.12).

Next, we perform a preliminary domain decomposition in the channel region alone, to motivate the elementary domain decomposition to follow. This highlights the effectiveness of the high field model in the channel region. Thus, in Fig. 5.4 (the whole region) and in Fig. 5.5 (zoomed-in pictures) we plot the comparison among the mid-region simulations of DD and HF, and the global kinetic simulation, at $vbias = 1.5V$. We perform the mid-region simulation for HF and DD with the boundary conditions provided by the kinetic simulation using $\mu = \mu(E)$ given by (2.12). We can see, especially in the zoomed-in pictures, that the high-field model has a better agreement with the kinetic simulations.

Finally, we perform the elementary domain decomposition by applying the low field drift diffusion model in [0,A] and [B,0.6], and the high field model in (A,B). Given the concentration n at the time level k, for points within [0,A] and [B,0.6], the update to the next time level is via the low field drift diffusion model. For points within (A,B), the update to the next time level is via the high field model. Interface coupling is implicit through the 7-point stencil of WENO schemes used for both models, as explained before.

The results of this elementary domain decomposition are shown in Fig. 5.6 (the whole region) and in Fig. 5.7 (zoomed-in pictures), for $vbias = 1.5V$, $A = 0.21$ and $B = 0.435$. We observe slight improvement of this elementary domain decomposition over the low field drift-diffusion model. For this device the low field drift-diffusion model with $\mu = \mu(E)$ as given in (2.12) is already a good model. We also observe that this elementary domain decomposition is numerically stable.

References

[1] H. U. Barenger and J. W. Wilkins, Ballistic structure in the electron distribution function of small semiconducting structures: General features and specific trends. *Phys. Rev. B*, **36**:1487–1502, 1987.

[2] C. Cercignani, I. M. Gamba, J. W. Jerome and C-W. Shu. Applicability of the high-field model: An analytical study based on asymptotic parameters defining domain decomposition. *VLSI DESIGN*, **8**:135–141, 1998.

[3] C. Cercignani, I. M. Gamba, J. W. Jerome and C-W. Shu. Applicability of the high-field model: A preliminary numerical study. *VLSI DESIGN*, **8**:275–282, 1998.

[4] C. Cercignani, I. M. Gamba and C. D. Levermore. High field approximations to Boltzmann-Poisson system boundary conditions in a semiconductor. *Appl. Math. Lett.*, **10**:111–117, 1997.

[5] E. Fatemi and F. Odeh. Upwind finite difference solution of the Boltzmann equation applied to electron transport in semiconductor devices. *J. Comput. Phys.*, **108**: 209–217, 1993.

[6] G. Frosali, C.V.M. van der Mee and S.L. Paveri-Fontana. Conditions for run–away phenomena in the kinetic theory of particle swarms, *J. Math. Physics* **30**:1177–1186, 1989.

[7] J. W. Jerome. *Analysis of Charge Transport: A Mathematical Study of Semiconductor Devices.* Springer, 1996.

[8] J. W. Jerome and C.-W. Shu. Energy models for one-carrier transport in semiconductor devices. *IMA Volumes in Mathematics and Its Applications*, **v59**, W. Coughran, J. Cole, P. Lloyd and J. White, editors, Springer-Verlag, 1994, pp.185-207.

[9] J. W. Jerome and C.-W. Shu. The response of the hydrodynamic model to heat conduction, mobility, and relaxation expressions. *VLSI DESIGN*, **3**:131–143, 1995.

[10] J. W. Jerome and C.-W. Shu. Transport effects and characteristic modes in the modeling and simulation of submicron devices. *IEEE Trans. Computer-Aided Design of Integrated Circuits and Systems*, **14**:917–923, 1995.

[11] G. Jiang and C.-W. Shu. Efficient implementation of weighted ENO schemes. *J. Comput. Phys.*, **126**:202–228, 1996.

[12] E. C. Kan, U. Ravaioli and T. Kerkhoven. Calculation of velocity overshoot in submicron devices using an augmented drift-diffusion model. *Solid-State Electr.*, **34**:995–999, 1991.

[13] F. Poupaud. Runaway phenomena and fluid approximation under high fields in semiconductor kinetic theory, *Z.Angew. Math. Mech.* **72**:359-372, 1992.

[14] F. Poupaud. Derivation of a hydrodynamic systems hierarchy from the Boltzmann equation, *Appl. Math. Lett.*, **4**:75-79, 1991.

[15] C.-W. Shu and S. Osher, Efficient implementation of essentially non-oscillatory shock capturing schemes II, *J. Comput. Phys.*, **83**:32–78, 1989.

[16] K. K. Thornber. Current equations for velocity overshoot. *IEEE Electron Device Lett.*, **3**:69–71, 1983.

[17] S.A. Trugman and A. J. Taylor, Analytic solution of the Boltzmann equation with applications to electron transport in inhomogeneous semiconductors, *Phys. Rev. B* **33**, 5575–5584 (1986).
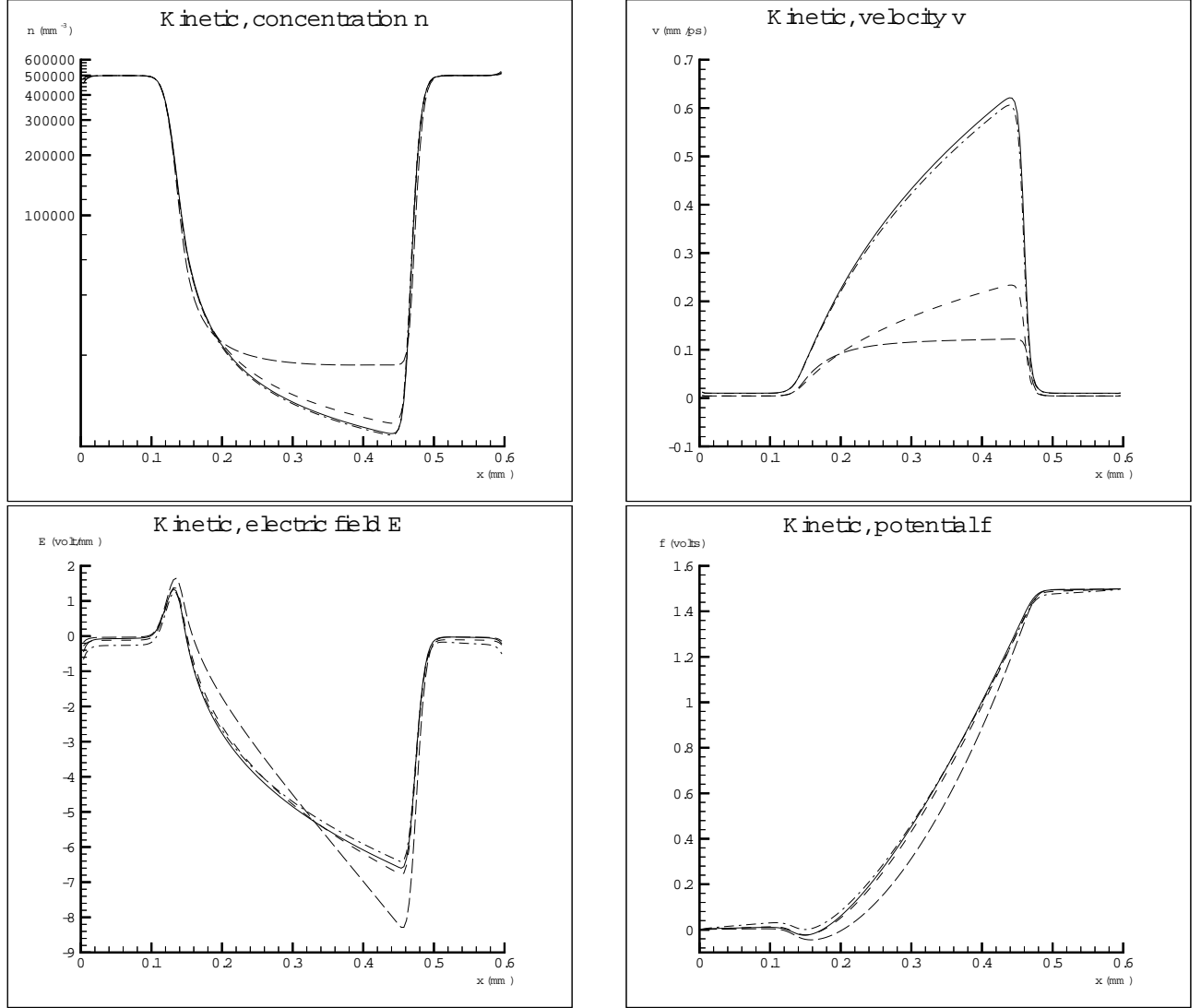
Figure 5.1: Kinetic simulation results of *vbias* = 1.5 volt with various assumptions on μ. Solid line: $\mu = .1323$; dashed line: $\mu = 0.0367$; dash-dotted line: $\mu = \mu(n_d)$ as given by (2.10); long dashed line: $\mu = \mu(E)$ as given by (2.12). Top left: the concentration n in μm^{-3}; top right: the velocity v in $\mu m/ps$; bottom left: the electric field E in *volts*/μm; bottom right: the potential ϕ in *volts*.
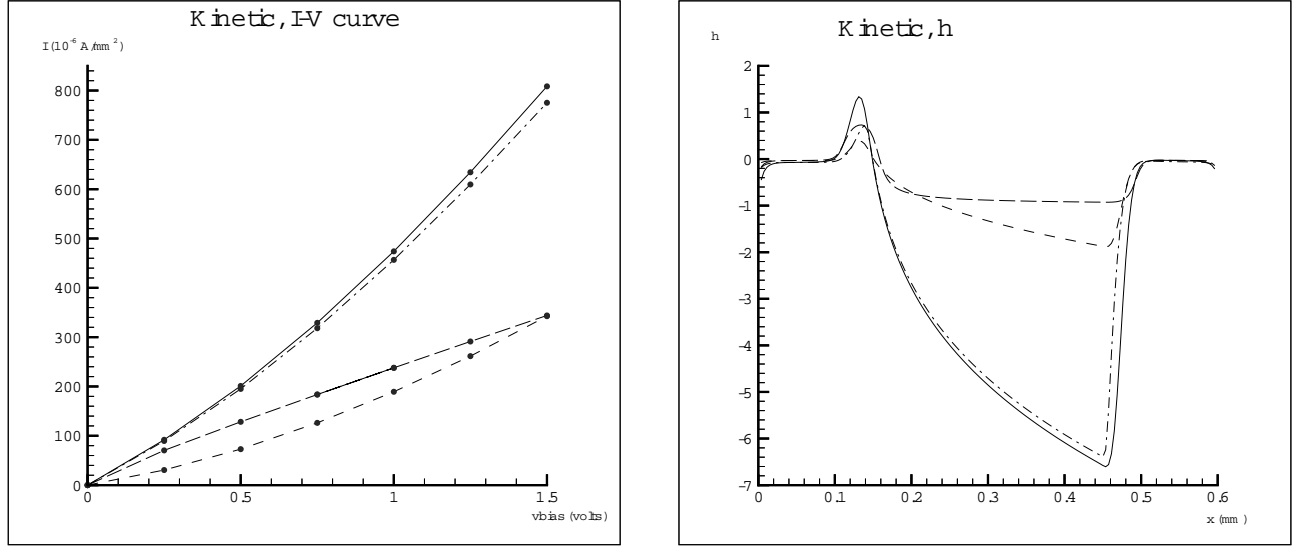
Figure 5.2: Kinetic simulation results with various assumptions on μ. Solid line: $\mu = .1323$; dashed line: $\mu = 0.0367$; dash-dotted line: $\mu = \mu(n_d)$ as given by (2.10); long dashed line: $\mu = \mu(E)$ as given by (2.12). Left: the I-V curve in $10^{-6} Amps/\mu m^2$ versus $volts$; right: the quantity η defined in (2.16) at $vbias = 1.5$ volt.

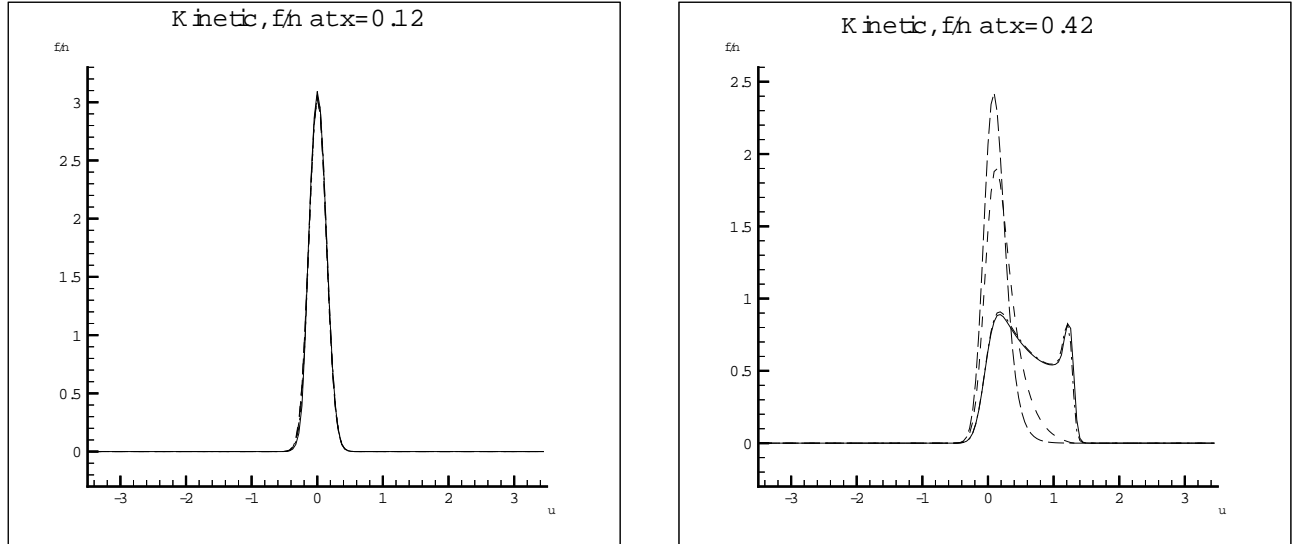Figure 5.3: The probability density function $f(x, u, t)/n(x, t)$ of the kinetic simulation with various assumptions on μ. Solid line: $\mu = .1323$; dashed line: $\mu = 0.0367$; dash-dotted line: $\mu = \mu(n_d)$ as given by (2.10); long dashed line: $\mu = \mu(E)$ as given by (2.12). Left: at $x = 0.12\mu m$; right: at $x = 0.42\mu m$.
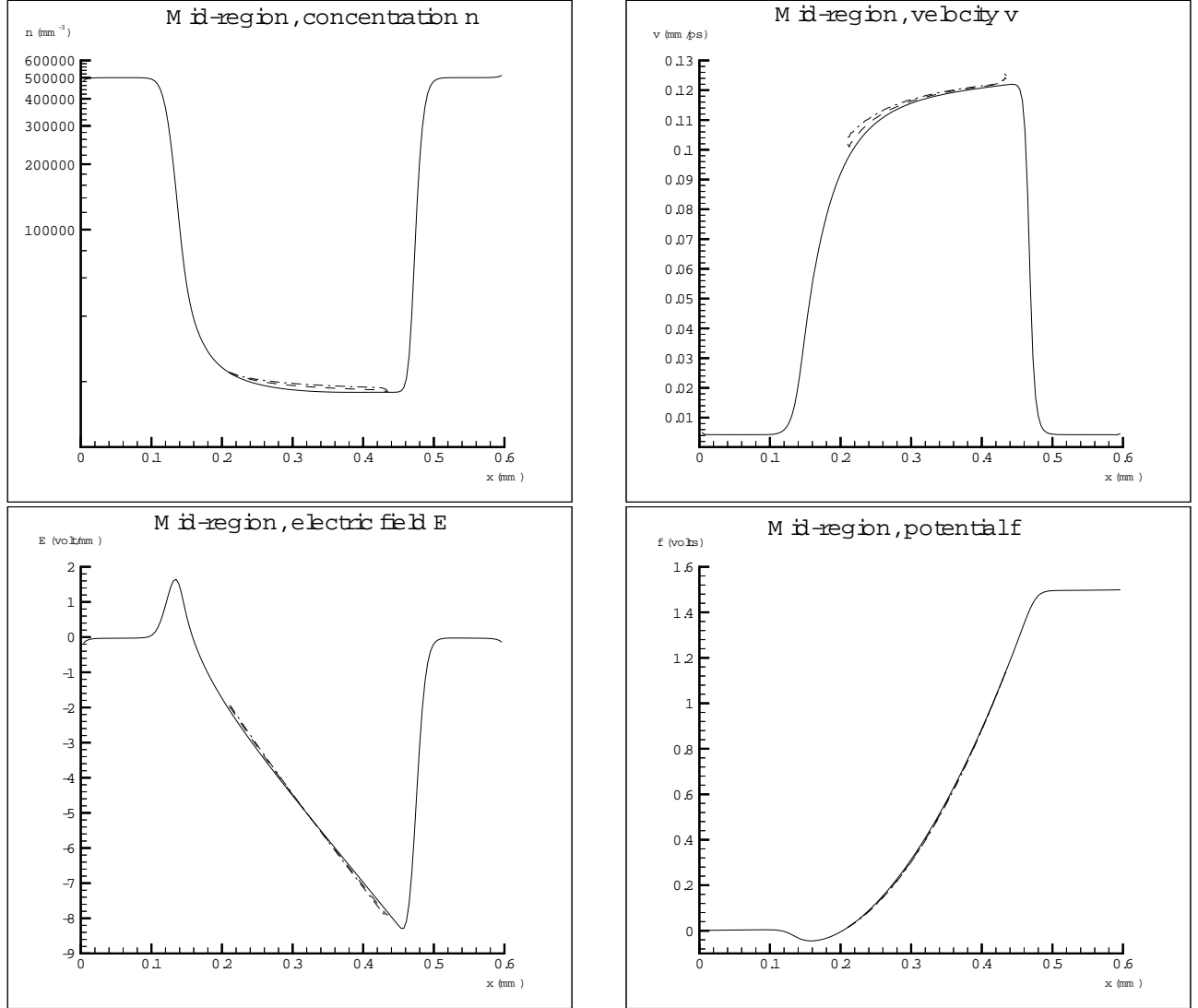
Figure 5.4: The global kinetic simulation (solid line), the mid-region HF simulation (dashed line), and the mid-region DD simulation (dash-dotted line). $\mu = \mu(E)$ for all simulations. The global kinetic simulation provides the boundary conditions for the mid-region HF and DD simulations. Top left: the concentration n in μm^{-3}; top right: the velocity v in $\mu m/ps$; bottom left: the electric field E in $volts/\mu m$; bottom right: the potential ϕ in $volts$.
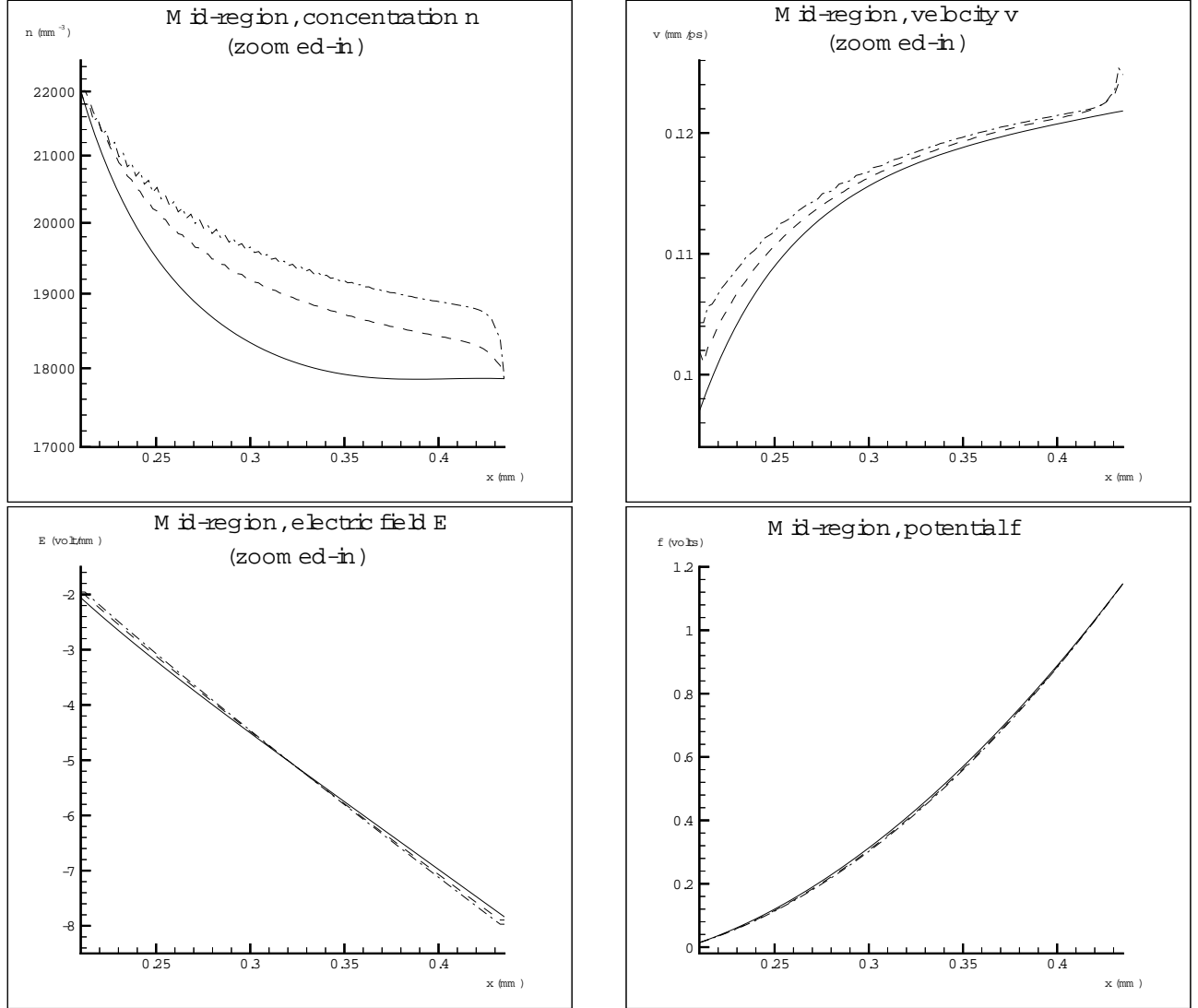
Figure 5.5: Zoomed-in pictures. The global kinetic simulation (solid line), the mid-region HF simulation (dashed line), and the mid-region DD simulation (dash-dotted line). $\mu = \mu(E)$ for all simulations. The global kinetic simulation provides the boundary conditions for the mid-region HF and DD simulations. Top left: the concentration n in μm^{-3}; top right: the velocity v in $\mu m/ps$; bottom left: the electric field E in $volts/\mu m$; bottom right: the potential ϕ in $volts$.
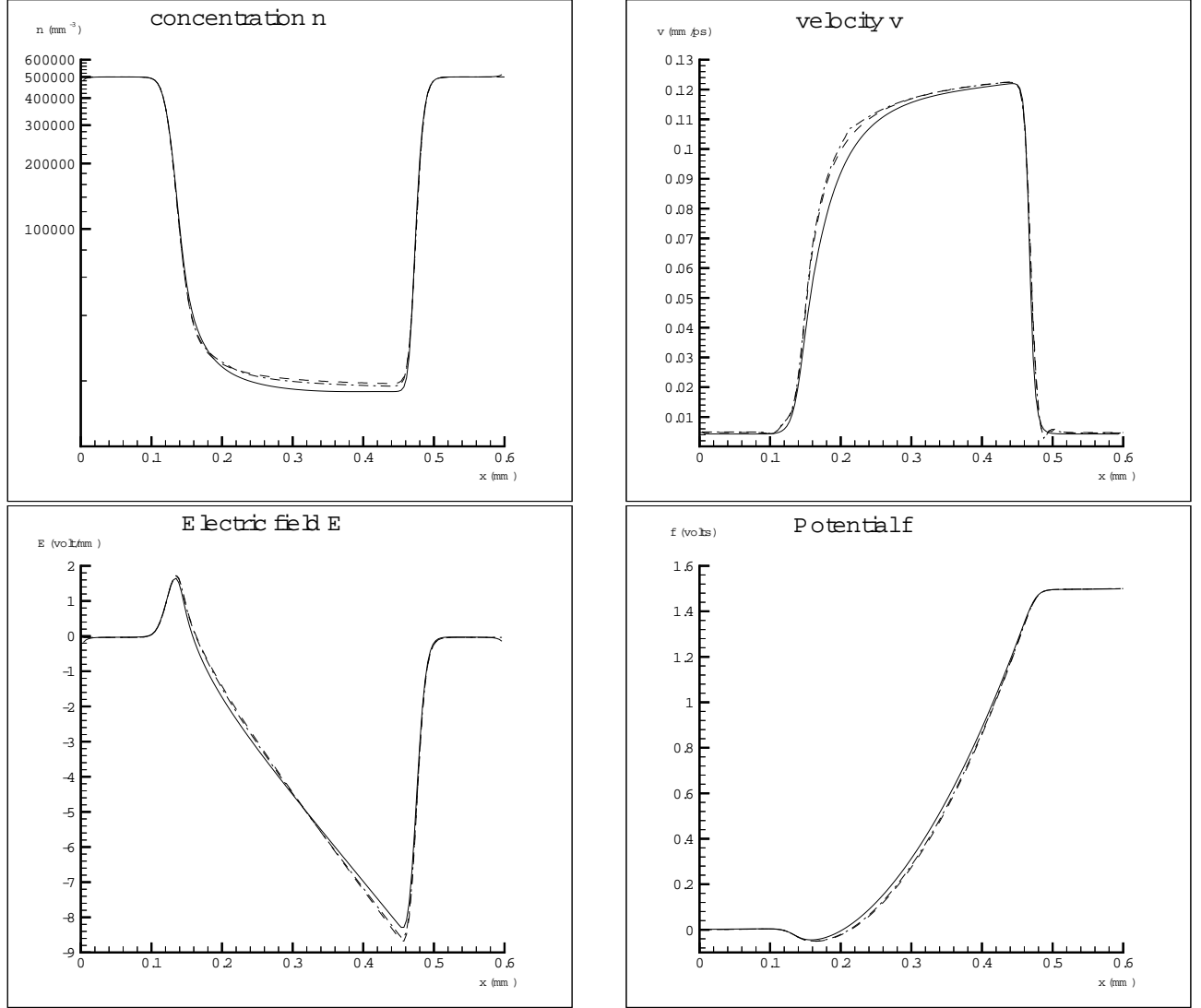
Figure 5.6: The global kinetic simulation (solid line), the global DD simulation (dashed line), and the elementary domain decomposition with the HF in (0.21,0.435) and DD otherwise (dash-dotted line). $\mu = \mu(E)$ for all simulations. Top left: the concentration n in μm^{-3}; top right: the velocity v in $\mu m/ps$; bottom left: the electric field E in $volts/\mu m$; bottom right: the potential ϕ in $volts$.
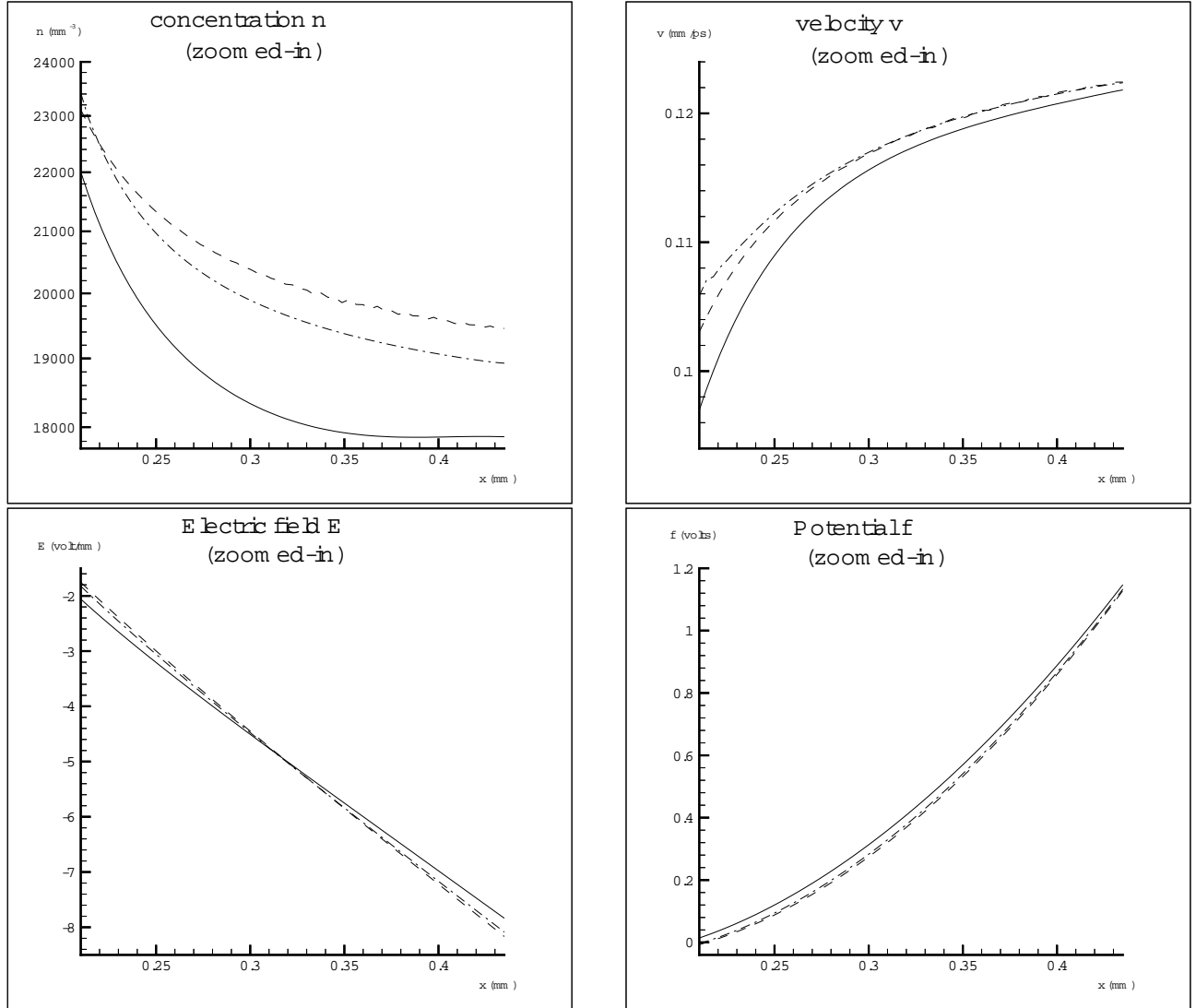
Figure 5.7: Zoomed-in pictures. The global kinetic simulation (solid line), the global DD simulation (dashed line), and the elementary domain decomposition with the HF in (0.21,0.435) and DD otherwise (dash-dotted line). $\mu = \mu(E)$ for all simulations. Top left: the concentration n in μm^{-3}; top right: the velocity v in $\mu m/ps$; bottom left: the electric field E in $volts/\mu m$; bottom right: the potential ϕ in $volts$.